Equations of state of matter for gasdynamic codes

Igor Lomonosov, Vadim Kim and Afanasii Ostrik

View Online

Export Citation

ARTICLES YOU MAY BE INTERESTED IN
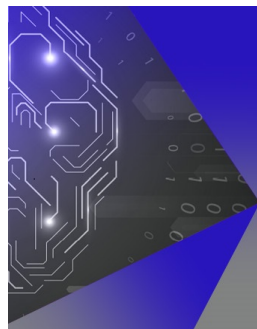
Equations of State of Matter for Gasdynamic Codes

Igor Lomonosov,[a] Vadim Kim,[b] and Afanasii Ostrik[c]

Institute of Problems of Chemical Physics of the Russian Academy of Sciences
Ac. Semenov avenue 1, Chernogolovka, Moscow region, 142432 Russian Federation

[a]*Corresponding author: director@icp.ac.ru*
[b]*Electronic mail: kim@ficp.ac.ru*
[c]*Electronic mail: ostrik@ficp.ac.ru*

Abstract. The equation of state is a fundamental characteristic of matter and is required in numerous studies and practically important problems of physics of high energy densities. The report discusses modern requirements for equations of state, theoretical and experimental methods for studying the thermodynamic properties of matter, various aspects of constructing wide-range equations of state and examples of using wide-range equations of state in modeling high-energy processes.

INTRODUCTION

Equation of state (EOS) describes fundamental thermophysical properties of matter [1]. This is a dependence between thermodynamic state quantities — is the main fundamental characteristic of a substance, making it possible to apply the general formal apparatus of thermodynamics and continuum dynamics to thermophysical objects and gas-dynamics energy processes of a different nature: from heat engines to transient phenomena at high energy densities. EOS is a "closing" relationship for the system of gas-dynamics equations, expressing in differential equations the most general laws of conservation of mass, momentum, and energy of matter, which, in turn, reflect the most fundamental properties of the symmetry of space–time (Noether's theorem) The laws of conservation of mass, momentum, and energy in the most general and compact mathematical form reflect the whole body of processes in nature, whereas an EoS complements this general formalism with qualitative characteristics of a particular substance: gas, liquid, crystal, and plasma, i.e., a whole variety of processes and phenomena in nature.

The interest in EOS of matter has always been high not only from the viewpoint of practical (technical or energetic) applications but also for understanding and describing processes and phenomena at high thermal energy densities. The advent of modern energy sources with a highly localized energy density, such as lasers, charged- and neutral-particle beams, shock waves, ultraintense electromagnetic waves, etc., has initiated laboratory studies of states of matter with earlier unreachable, extremely high pressures and temperatures, corresponding to new regions of the phase diagrams of matter. This substantially extended the community of scientists interested in physic of high energy-density physics [1, 2, 3]. The fast progress in numerical methods for new peta- and exaflop computers necessitated the development of efficient difference schemes for calculating transient gasdynamics phenomena [4, 5, 6, 7, 8], which significantly raised the requirements to the adequate and detailed description of thermodynamic properties of matter, because the accuracy of gas-dynamics calculations is determined not only by the errors of solving conservation equations but, first and foremost, by errors in the EOS of a substance.

So, EOS is a necessary part of numerical modeling of high-energy processes that controls the specificity and accuracy of numerical calculations of transient processes. As a result, modern complexes and software packages must have libraries and databases of modern EOS for numerous materials and chemical compounds to describe their behavior in a wide range of the phase diagram.

EOS: THEORY AND EXPERIMENT

The current state of the problem of a theoretical description of thermodynamic properties of matter at high pressures and high temperatures is given in a set of publications (see refs. [1, 9, 10] and references therein). In spite of the significant progress achieved in predicting EOS information accurately in solid, liquid, and plasma states with the use of the most sophisticated "ab initio" computational approaches (classic and quantum methods of self–consisted field, diagram technique, Monte–Carlo, and molecular dynamics methods), the disadvantage of these theories is their regional character [1, 9, 10]. For example [1], the Schrodinger equation is solving for crystal at $T = 0$ K, while integral equations relate pair interactive potential and pair correlation function for liquid and chemical potentials are used in the "chemical" model of plasmas.

The range of applicability of each method is local and, rigorously speaking, no single one of them provides for a correct theoretical calculation of thermodynamic properties of matter on the whole phase plane from the cold crystal to the liquid and hot plasmas [1, 9]. The principal problem here is the need to account correctly for the strong collective interparticle interaction in disordered media, which presents special difficulties in the region occupied by dense, disordered, nonideal plasmas [1, 9].

In this case, experimental data at high pressures and high temperatures are of particular significance, because they serve as reference points for theories and semi-empirical models. Data obtained with the use of dynamic methods (see [2, 11, 12, 13, 14, 15] and references therein) are of the importance from the practical point of view. Shock–wave methods permit to study a broad range of the phase diagram from the compressed hot condensed states to dense strongly coupled plasma and quasi–gas states. Detailed presentations of shock–wave methods to investigate high dynamic pressures is given in monographs [1, 2, 10, 11] and reviews [16, 17].

The available experimental information is shown in Fig. 1 on a 3D, relative volume–temperature–pressure surface for aluminum, calculated by a semi–empirical multi–phase EOS [18, 19]. The experimental data on the shock compression of solid and porous metals, as well as isentropic expansion, covers nine orders of magnitude in pressure and four in density. In a viscous compression shock termed the shock front, the kinetic energy of the oncoming flow is converted to the thermal energy of the compressed and irreversibly heated medium. This way of shock compression, see the principal Hugoniot in Fig. 1, has no limitations in the magnitude of the pressure obtained but is bounded by the short lifetimes of the shock-compressed substance. That is why the techniques employed for the diagnostics of these states should possess a high ($\sim 10^{-6} - 10^{-9}$ s) temporal resolution. When a stationary shock-wave discontinuity propagates through a material, the conservation laws of mass, momentum, and energy [2] are obeyed at its front. These laws relate the kinematic parameters, the shock wave velocity D and the mass material velocity U behind the shock front, with thermodynamic values — the specific internal energy E, the pressure P, and the specific volume V:

$$\frac{V_0}{V} = \frac{D}{D-U}, \ \ P = P_0 + \frac{DU}{V_0}, \ \ E = E_0 + \frac{1}{2}(P+P_0)(V_0-V). \tag{1}$$

Here the subscript 0 indicates the parameters of the immobile material ahead of the shock front. These equations permit determining the hydro- and thermodynamic characteristics of a shock-compressed mate rial upon recording any two of the five parameters E, P, V, D, and U, which characterize the shock discontinuity. Determined most easily and precisely by standard techniques is the shock velocity D. The choice of the second recorded parameter depends on specific experimental conditions. The "arrest" and "reflection" (impedance–matching) methods are using [2] for condensed materials. Depending on experimental setup, either shock front velocities in target and etalon materials or the shock front velocity in target and the impactor velocity are measuring. Today, a wide variety of ways of generating intense shock waves is employed in dynamic experiments. These are chemical, nuclear, and electric explosions; pneumatic, gun powder, and electrodynamic guns; concentrated laser and soft X-ray radiation; and relativistic electron and ion beams [1, 9, 10].

The first published shock–wave data were obtained for metals in the megabar (1 Mbar= 100 GPa) [20] and multimegabar [21, 22] pressure range using explosive drivers. Higher pressures of tens megabars have been accessed by spherical cumulative systems [23, 24] and by underground nuclear explosions [25, 26]. Maximum pressures of 400 TPa [27] were also reported for aluminum through the use of nuclear explosion. Note, that data obtained by impedance–matching techniques require the knowledge of the EOS for a standard material. Previously a monotonic approximation of the shock adiabat of lead between the traditional region of pressures ≤ 10 Mbar to Thomas–Fermi calculations was used for the standard [25, 26]. It seems that iron, for which absolute Hugoniot measurements have been reported to pressures of 100 Mbar [28, 29], is now the best etalon material.

The extension of the phase diagram data to greater relative volumes, in comparison with the principal Hugoniot, is achieved with shock compression of porous samples [2]. Nevertheless, difficulties in fabricating highly porous targets and non–uniform material response of the porous sample to shock loading imposes a practical limit to the minimum density of a specimen. The method of isentropic expansion of shocked matter, depending on the magnitude of the shock pressure and, consequently, the entropy provided, produces in one experiment transitions from a hot metallic liquid shocked state , to a strongly coupled plasma, then to a two–phase liquid–gas region, and to a Boltzmann's weakly ionized plasma, and finally to a nearly ideal gas [2, 9, 11].

Another important case of self-similar gas dynamic flow is the centered Riemann rarefaction wave. In experiments involving determination of isentropic expansion curves for a shock-compressed material, the states in the centered

dumping wave are described by Riemann integrals [2]:

$$V_S = V_H + \int_{P_S}^{P_H} \left(\frac{dU}{dP}\right)^2 dP, \ E_S = E_H - \int_{P_S}^{P_H} P \left(\frac{dU}{dP}\right)^2 dP, \tag{2}$$

where indexes S and H relate to isentrope and shock adiabat, correspondingly, and integrals are calculated along the measured isentrope $P = P_S(U)$.

These measurements of release isentropes of shocked materials are of especial importance. The adiabatic expansion of a substance, see curves s in Fig. 1, precompressed to megabar pressures by a shock wave, permits investigating an interesting plasma parameter domain located between a solid and a gas, including the metal—dielectric transition region and the high-temperature portion of the boiling curve of metals with their critical point [9, 30]. Since the metallic bond energy is rather high, the parameters of the critical points of metals are extremely high (4.5 kbar and 8000 K for aluminum, 15 kbar and 21000 K for tungsten [9]) and unattainable for static experimental techniques. That is why until recently the critical point characteristics were measured only for three of all metals, which account for $\sim 80\%$ of the elements of the Periodic Table [9]. On the other hand, because the critical temperatures of metals are high and are comparable to their ionization potentials, metals in a near-critical state vaporize directly to an ionized state and not to a gas, as is the case in the rest of the chemical elements. This circumstance may lead to exotic "plasma" phase transitions predicted for metallization by Ya. B. Zel'dovich and L. D. Landau [31] and other theorists for strongly compressed Coulomb systems (see Refs. [9, 32, 33, 34] and references therein). Such results traverse states in the intermediate region between the solid state and gas, occupied by a hot dense metallic liquid and strongly coupled plasma [9, 11], which is a region poorly described by theory. Experimentally studied release isentropes for copper have as initial high energy states solid, and melted, and compressed liquid metal. The range of thermodynamic parameters covered in the adiabatic expansion process for these states is extremely wide (Fig. 1), covering five orders of magnitude in pressure and two orders of magnitude in density. It extends from a highly compressed metallic liquid, characterized by a disordered arrangement of ions and degenerate electrons, to a quasi–nonideal Boltzmann plasma and a rarefied metallic vapor. Upon expansion of the system, the degree of degeneracy of the electronic subsystem is decreased and a marked rearrangement of the energy spectrum of atoms and ions occurs. A partial recombination of the dense plasma also takes place. In the disordered electron system a "metal–insulator" transition takes place and a nonideal (with respect to different forms of interparticle interactions) plasma is formed in the vicinity of the liquid–vapor equilibrium curve and the critical point. Where the isentropes enter the two–phase liquid–vapor region evaporation occurs; on the gas–side condensation occurs [9, 11, 18].

Note, that typical shock–wave measurements allow determination of only caloric properties of matter, viz. the dependence of the relative internal energy on pressure and volume as $E = E(P,V)$. The potential $E(P,V)$ is not complete in the thermodynamic sense and a knowledge of temperature T or entropy S is required for completing the thermodynamic equations and calculating first and second derivatives, such as the heat capacity, the sound velocity and others [1].

Only a few temperature measurements in shocked metals are available [35], as well as analogous measurements in release isentropic waves [18]. This information is of great importance in view of a limitation of purely theoretical calculation methods. From this point of view, thermodynamically complete measurements obtained with the use of the isobaric expansion (IEX) technique [36] are of a special significance. In this method metal is rapidly heated by a powerful pulsed current, then expands into an atmosphere of an inertial gas maintained at constant pressure. This data range in density form solid to the critical point and intersect, therefore, the release isentrope data for metals (see Fig. 1). Data on slow electric discharge in metallic foil, "Enceinte à Plasma Isochore" (EPI) [37], are attributed to case of the isochoric heating and occupy the supercritical domain on the phase diagram.

The region between principal shock adiabat and isotherm can be accessed with use of the isentropic compression technique. This method allows one to obtain simultaneously high pressure and high densities in the material under study. In practice the sample is loaded by a magnetically driven impactor or by a sequence of reverberating shock waves in a multi–step compression process.

The final conclusion is that shock–wave techniques allow one to investigate material properties in very wide region of the phase diagram — from compressed solid to hot dense liquid, plasma, liquid–vapor, and quasi–gas states. Though the resulting high pressure, high and temperature information covers a broad range of the phase diagram, it has a heterogeneous character and, as a rule, is not complete from the thermodynamic point of view. Its generalization can be done only in the form of a thermodynamically complete EOS.
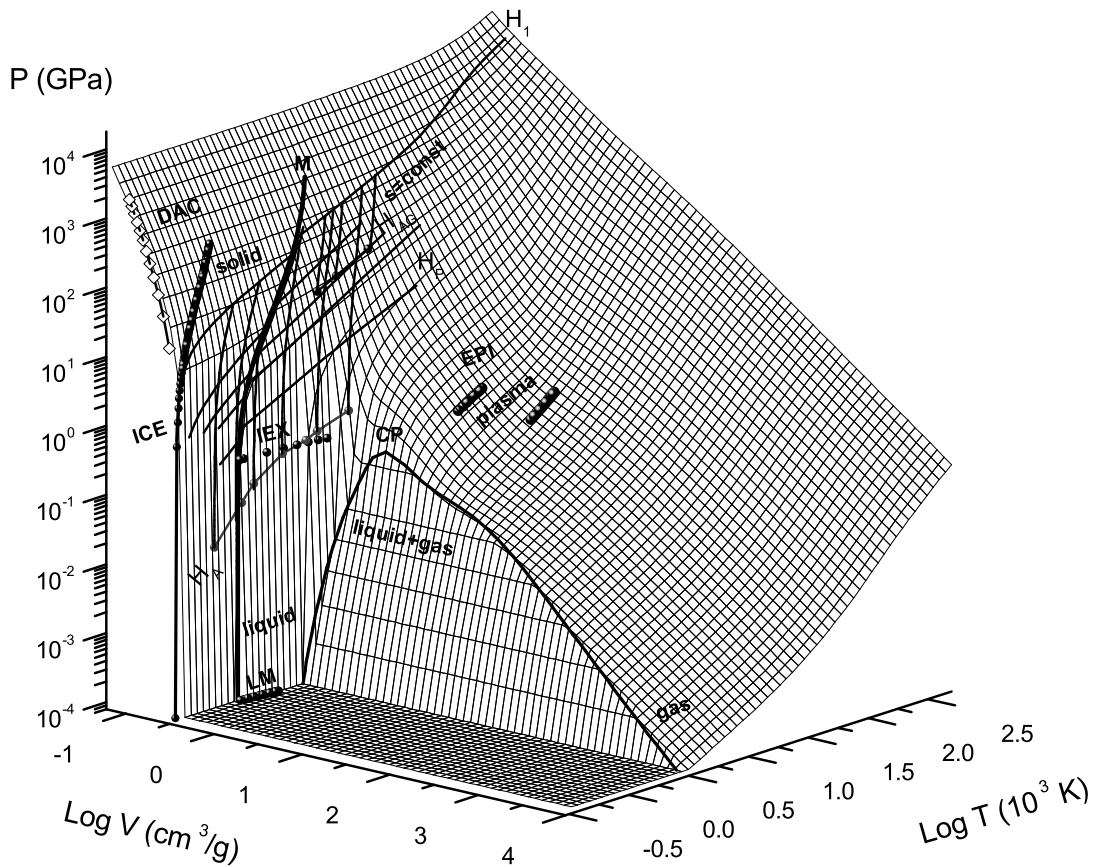
FIGURE 1. Generalized 3D volume–temperature–pressure surface for aluminum. M—melting region; R—boundary of two–phase liquid–gas region with the critical point CP; H_1 and H_p—principal and porous Hugoniots; H_A and H_{AG}— shock adiabats of air and aerogel; DAC—diamond–anvil–cells data; ICE—isentropic compression experiment; IEX—isobaric expansion data; S—release isentropes. Phase states of the metal are also shown.

EOS PROBLEM, DEMANDS AND FORMULATION

Constructing adequate EOS of a substance is a major challenge (see [1, 17] and references therein). According to [1], modern models of EOS are constructed either from experimental results or by methods of statistical physics. The main difficulty on the way to a consistent theoretical calculation of the EOS of a substance by methods of statistical physics is the necessity to correctly take into account the complex structure of interparticle interaction in the quantum-mechanical many-body problem with arbitrary coupling constants and any type of statistics. Therefore, the calculations usually employ simplified models, the applicability of which is limited and established in each particular case on the basis of either the internal characteristics of the model or by a comparison with more accurate solutions or experimental results. The latter way is obviously more constructive, because there are numerous examples (the van der Waals theory, integral equations, nonideal plasma, etc.) in which the actual applicability of models goes significantly beyond the bounds dictated by the smallness of the corresponding dimensionless parameters and criteria.

In the next stage of the development of thermodynamic models, the existing experimental data are utilized to choose the basic numerical parameters in the functional dependences based on exact solutions or simplified models. The semiempirical models obtained in this manner are used to describe and formulate an adequate model of the zero approximation in especially complex situations (liquids, solids, and dense electromagnetic and quark-gluon plasma) not allowing one to separate a small parameter of the perturbation theory. The success in developing semiempirical models is verified by both the quality of describing a wide variety of different experimental data and the possibility of extrapolation calculations. It is clear that, for semiempirical EoSs, the experiment is not only a necessary complement

but also the actual basis of their existence.

Despite the utmost generality and internal consistency of the formal apparatus of continuum mechanics, numerical calculations of particular phenomena with chosen EOS have their specific features. Upon a typical high-power energy release, matter undergoes complex thermodynamic processes. The energy release gives rise to a three-dimensional gas-dynamics flow, characterized by large gradients of thermodynamic quantities. It involves different phases: from a crystal to a hot liquid and to an evaporated and ionized substance. The numerical simulation of such processes requires the use of wide-range EOS. In most phenomena of practical interest, macroscopic quantities characterizing the state of a substance vary rather slowly as compared to the rates of relaxation processes leading to thermodynamic equilibrium. Under such conditions, particles of a continuous medium remain in a state close to thermodynamic equilibrium. In an adiabatic motion (in the absence of heat transfer), the equilibrium states of gas particles can be described by entropy or the internal energy as functions of specific volume and pressure $S(V,P)$ and $E(V,P)$. In the general nonadiabatic case, the equation involves temperature, which should also be related to pressure and specific volume, e.g., in the form $P(V,T)$. As was noted above, all state functions can be obtained from one potential (internal energy E, enthalpy H, Helmholtz free energy F, Gibbs function G) defined as a function of the corresponding variables: $E(S,V)$, $H(S,V)$, $F(V,T)$ and $G(P,T)$. Thus, it is natural to understand that constructing an equation of state is specifying one of these dependences. However, in practice [1], constructing an equation of state is often understood as a less complete description of the properties of a substance (e.g., constructing a caloric equation in the form $P(V,E)$).

The main goal of EOS development is its usage in gas dynamic codes. The experience of numerical modeling puts physical and mathematical demands and limitations to EOS.

This is wide range of applicability, i.e. EOS must describe thermodynamic properties in solid, liquid and plasma states. EOS also must be continuous and smooth in each phase. EOS for each phase must provide for mathematic conditions of resistance to compression (at $P(T = const) \rightarrow \infty$ one has $V \rightarrow 0$), stability of the heat conductivity ($C_V = (\partial E/\partial T)_V > 0$), existence of acoustic perturbations ($C_S = (\partial P/\partial \rho)_S^{1/2} > 0$) and stability of shock compression waves ($(\partial^2 P/\partial V^2)_T > 0$). The scalability means that new experimental or theoretical information can be easily implemented in EOS. Finally, the EOS part in gas dynamic calculations must be minimal. It is not simple to satisfy simultaneously all of these demands. This fact explains a great amount of EOS models.

EOS models are given by thermodynamically complete potentials. The free energy thermodynamic potential $F = E - TS$ is most suitable, its complete differential is

$$dF = -SdT - PdV \tag{3}$$

The knowledge of $F(V,T)$ of the uniform system under condition of thermodynamic equilibrium allows one to determine partial derivatives which are used to obtain measured thermodynamic functions and other potentials. Let us show it on example of the free energy:

$$P(V,T) = -\left(\frac{\partial F(V,T)}{\partial V}\right)_T = -F_V \tag{4}$$

$$S(V,T) = -\left(\frac{\partial F(V,T)}{\partial T}\right)_V = -F_T \tag{5}$$

$$C_V(V,T) = T\left(\frac{\partial S(V,T)}{\partial T}\right)_T = -T \times F_{TT} \tag{6}$$

$$C_P(V,T) = T\left(\frac{\partial S(V,T)}{\partial T}\right)_P = T\left(\left(\frac{\partial S}{\partial T}\right)_V - \frac{\left(\frac{\partial P}{\partial T}\right)_V \left(\frac{\partial S}{\partial V}\right)_T}{\left(\frac{\partial P}{\partial V}\right)_T}\right) = T\left(-F_{TT} + \frac{F_{VT}^2}{F_{VV}}\right) \tag{7}$$

$$C_T^2(V,T) = -V^2\left(\frac{\partial P(V,T)}{\partial V}\right)_T = -V^2 F_{VV} \tag{8}$$

$$C_S^2(V,T) = -V^2 \left(\frac{\partial P(V,T)}{\partial V} \right)_S = -V^2 \left(\left(\frac{\partial P}{\partial V} \right)_T - \frac{\left(\frac{\partial S}{\partial V} \right)_T \left(\frac{\partial P}{\partial T} \right)_V}{\left(\frac{\partial S}{\partial T} \right)_V} \right) = -V^2 \left(-F_{VV} + \frac{F_{VT}^2}{F_{TT}} \right) \tag{9}$$

Here in formulas (4), (5), (6),(7), (8), (9) P, S, C_V, C_P, C_T and C_S are pressure, entropy, heat capacities at constant volume and pressure, isothermal and isentropic sound velocities, correspondingly.

Considering a mixture of two phases *1* and *2* of matter at given pressure and temperature also under condition of thermodynamic equilibrium with relative parts ξ and $(1-\xi)$, it is easy to obtain

$$V = \xi V_1 + (1-\xi)V_2 \tag{10}$$

$$S = \xi S_1 + (1-\xi)S_2 \tag{11}$$

$$\xi = \frac{V - V_1}{V_2 - V_1} = \frac{S - S_1}{S_2 - S_1} \tag{12}$$

Corresponding differentials are

$$dV = \xi dV_1 + (1-\xi)dV_2 + (V_1 - V_2)d\xi \tag{13}$$

$$dS = \xi dS_1 + (1-\xi)dS_2 + (S_1 - S_2)d\xi \tag{14}$$

$$d\xi = \frac{1}{V_2 - V_1}(\xi dV_1 + (1-\xi)dV_2) \tag{15}$$

The partial volume derivative is

$$F_{VV} = 0 \tag{16}$$

while the mixtured derivative is derived by Clausius–Clapeyron law

$$F_{VT} = \frac{dP}{dT} = \frac{S_2 - S_1}{V_2 - V1} \tag{17}$$

Using differentials of pressure $dP = \left(\frac{\partial P}{\partial V} \right)_T dV + \left(\frac{\partial P}{\partial T} \right)_V dT$ and of entropy $dS = \left(\frac{\partial S}{\partial V} \right)_T dV + \left(\frac{\partial S}{\partial T} \right)_V dT$ one can obtain

$$\frac{dV}{dT} = \frac{\frac{dP}{dT} - \left(\frac{\partial P}{\partial T} \right)_V}{\left(\frac{\partial P}{\partial V} \right)_T} \tag{18}$$

$$\frac{dS}{dT} = \left(\frac{\partial S}{\partial T} \right)_V + \left(\frac{\partial S}{\partial V} \right)_T \frac{dV}{dT} \tag{19}$$

Equations (14), (15), (17), (18), (19) allows one to determined the complete derivative of the mixture (here $A' = \frac{dA}{dT}$)

$$\frac{dS}{dT} = \xi S_1' + (1-\xi)S_2' - \frac{S_1 - S_2}{V_1 - V_2}(\xi V_1' + (1-\xi)V_2') = \xi \left(S_1' - V_1' \frac{dP}{dT} \right) + (1-\xi)\left(S_2' - V_2' \frac{dP}{dT} \right) \tag{20}$$

and the partial one

$$-F_{TT} = \left(\frac{\partial S}{\partial T}\right)_V = \xi \left[\left(\frac{\partial S}{\partial T}\right)_V + \left(\left(\frac{\partial P}{\partial T}\right)_V - \frac{dP}{dT}\right)\frac{\frac{dP}{dT} - \left(\frac{\partial P}{\partial T}\right)_V}{\left(\frac{\partial P}{\partial V}\right)_T}\right]_1 + $$

$$+ (1-\xi)\left[\left(\frac{\partial S}{\partial T}\right)_V + \left(\left(\frac{\partial P}{\partial T}\right)_V - \frac{dP}{dT}\right)\frac{\frac{dP}{dT} - \left(\frac{\partial P}{\partial T}\right)_V}{\left(\frac{\partial P}{\partial V}\right)_T}\right]_2 = $$

$$= \xi \left[-F_{TT} + \frac{\left(\frac{dP}{dT} + F_{VT}\right)^2}{F_{VV}}\right]_1 + (1-\xi)\left[-F_{TT} + \frac{\left(\frac{dP}{dT} + F_{VT}\right)^2}{F_{VV}}\right]_2 \quad (21)$$

where indexes relate to thermodynamic functions of phases *1* and *2*.

Obviously, one can not use multi-phase EOS in gas dynamic codes directly. Indeed, thermodynamic derivatives are easily determined for the case of the uniform physical system, see Eqs. (6)-(9). These equations become much more complicated in the case of thermodynamically equilibrium two-phase system, see Eqs. (10)-(21). Note, that it is also necessary to know relative parts ξ and $(1-\xi)$ of these phases. So the use of EOS in tabulated form is an efficient decision, which provides for good accuracy of EOS description and high performance of gas dynamic computations. The generation of tables using united EOS model [11, 19, 38, 39] guarantees the self consistency of thermodynamic functions.

As it seen from this consideration, in practice wide-range EOS means multi-phase EOS and, finally, tabulated EOS.

RESULTS OF COMPUTER MODELING

We present in this section results of numerical modeling done with the original 3D parallel code, see for details [40]. It is based on "finite-size particle in cell" method developed for numerical modeling of processes at high energy density. It uses the Lagrangian-Eulerian representation of media which allows one to match contact and free surfaces and to calculate flows with strong deformations. Efficient models of thermodynamic properties, elastic–plastic deformation and fragmentation have been employed in the gas dynamic code adapted for parallel computations.

An impact of lead sphere (1.5 cm diameter, 20 g mass) on lead plate (0.63 cm thickness) has been investigated experimentally [41]. These data are of especial interest because the experimental x–ray shot at 30 μs fixed the spatial distribution of impactor and plate densities. It allows one to compare directly computational and experimental results. The high value of impact velocity results to melting of both impactor and plate with further significant evaporating during expansion. Earlier 2D numerical modeling of this problem [42] demonstrated the paradox result—the best description was obtained with the use of most simple EOS model.

3D numerical modeling of experiment [41] has been carried out with multi–phase [11] and caloric [17] EOS for lead in hydrodynamic approach.
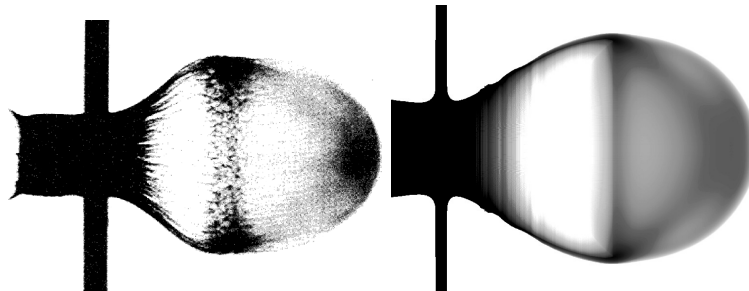

FIGURE 2. Sphere on plate impact for Pb: experimental (left) and computed (right) x-ray photograph of the debris cloud at 30 μs.

The spatial distribution of density at 30 μs obtained in numerical modeling with use of multi–phase EOS has been integrated. This profile is compared with experimental one [41] on Fig. 2, the agreement in form and sizes is good.

On the transmission image of this process, the darker areas correspond to higher integrated density and the calculated shape and size of the cloud of fragments and the density distribution are in a good agreement with the experiment. The results of calculations with the caloric EOS showed significant deviations from the experimental X-ray diffraction pattern and from the time distributions of density and pressure obtained with the multiphase EOS.

These effects have a physical explanation from the analysis of thermodynamic path of the impact and release processes. According to multi–phase EOS [11], lead is liquid after impact. Its entropy is practically equal to the entropy of the critical point, so it strongly evaporates with positive pressure during expansion along the release isentrope. The caloric EOS [17] does not provide for correct description of the vaporization effect at low densities. Moreover, it produces negative pressures at specific volumes V=0.1 g/cm^3 and higher which corresponds to two–phase liquid–gas region on the phase P—V–diagram. So, the use of caloric EOS results to occurring of significant regions of negative pressures in expanding material, up to its mechanic failure. The use of multi–phase EOS results to a failure in solid state, while the expansion of material with high specific entropy leads to its evaporating.

From the analysis of the calculated pressure and density distributions and comparison with the experimental X-ray diffraction pattern, we conclude that the results of numerical simulation using the multiphase EOS, which is more physically justified, correctly describe the experimental data and physical processes upon a high-velocity impact.
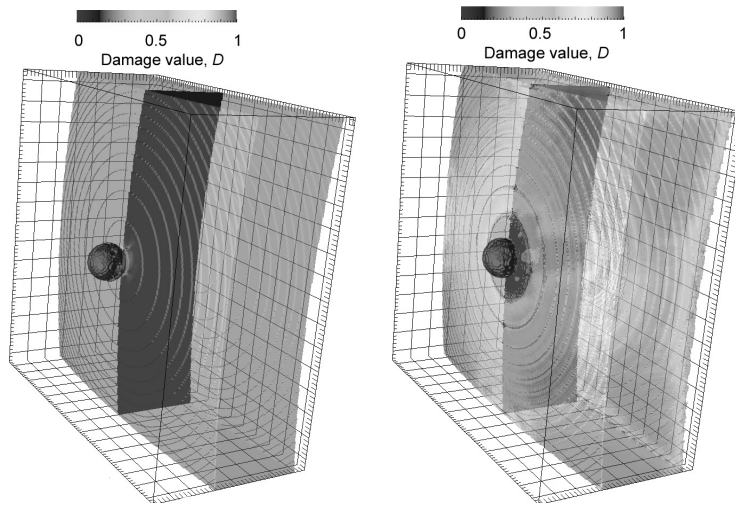

FIGURE 3. 3D chondrite sphere impact on silica wall: results of computer modeling. Damage value distribution at 0.1 μs (left) and 2 μs (right).

Another example of numerical modeling corresponds to an impact of chondrite asteroid on Earth surface. Simplified caloric EOS [43] developed for chondrite was implemented in the framework of 3D gas dynamics computer code as well as previously developed EOS for silica. An impact of chondrite sphere (0.8 m diameter, 2000 kg mass) on silica plate (2 m thickness) has been investigated in 3D. Three dimensional surfaces of material damage value distribution at 0.1 μs and 2.0 μs are on Fig. 3. These calculations have been done as model tests of high-velocity asteroid impact.

CONCLUSION

The problem of developing efficient EOS for using in numerical modeling of of high-energy processes has been considered. The general demands to EOS are formulated and discussed. The necessity to generalize the experimental and theoretical information contained in local sections of the phase diagram into a semiempirical EOS has been demonstrated. Results of numerical modeling of high-velocity impacts calculated with realistic EOS, have been presented and discussed.

ACKNOWLEDGMENTS

REFERENCES

1. V. E. Fortov, *Thermodynamics and equations of state for matter: from ideal gas to quark-gluon plasma* (World Scientific, Singapore, 2016).
2. Y. B. Zeldovich and Y. P. Raizer, *Physics of Shock Waves and High–Temperature Hydrodynamic Phenomena* (Academic Press, New York, 1966).
3. D. Henderson, ed., *Frontiers in High Energy Density Physics* (National Research Council, Nat. Acad. Press, Washington, 2003).
4. E. S. Hertel, R. L. Bell, M. G. Elrick, A. V. Farnsworth, G. I. Kerley, J. M. McGlaun, S. V. Petney, S. A. Silling, P. A. Taylor, and L. Yarrington, "CTH: A software family for multi-dimensional shock physics analysis," in *Shock Waves @ Marseille I: Hypersonics, Shock Tube & Shock Tunnel Flow*, edited by R. Brun and L. Z. Dumitrescu (Springer Berlin Heidelberg, Berlin, Heidelberg, 1995) pp. 377–382.
5. A. Robinson, T. Brunner, S. Carroll, R. Drake, C. Garasi, T. Gardiner, T. Haill, H. Hanshaw, D. Hensinger, D. Labreche, *et al.*, "ALEGRA: An arbitrary Lagrangian-Eulerian multimaterial, multiphysics code," in *46th AIAA Aerospace Sciences Meeting and Exhibit* (2008) p. 1235.
6. A. Ferrari, M. Dumbser, E. F. Toro, and A. Armanini, "A new 3D parallel SPH scheme for free surface flows," Computers & Fluids **38**, 1203–1217 (2009).
7. V. A. Gasilov, A. S. Boldarev, S. V. Dyachenko, O. G. Olhovskaya, E. L. Kartasheva, S. N. Boldyrev, G. A. Bagdasarov, I. V. Gasilova, M. S. Boyarov, and V. A. Shmyrov, "Package of applied programs MARPLE3D for modeling on high-perfromance computers of pulsed magneto-accelerated plasmas," Mat. Model **24**, 44–87 (2012).
8. S. H. Langer, I. Karlin, and M. M. Marinak, "Performance characteristics of HYDRA–a multi-physics simulation code from LLNL," in *International Conference on High Performance Computing for Computational Science* (Springer, 2014) pp. 173–181.
9. V. Fortov, I. Yakubov, and A. Khrapak, *Physics of Strongly Coupled Plasma* (Clarendon Press, Oxford, 2006).
10. V. E. Fortov, *Extreme states of matter: on Earth and in the Cosmos* (Springer, Berlin, Heidelberg, 2011).
11. A. V. Bushman, G. I. Kanel, A. L. Ni, and V. E. Fortov, *Thermophysics and Dynamics of Intense Pulse Loadings* (Taylor&Fransis, London, 1993).
12. R. G. McQueen, S. P. Marsh, J. W. Taylor, J. N. Fritz, and W. J. Carter, "The equation of state of solids from shock wave studies," in *High Velocity Impact Phenomena*, edited by R. Kinslow (Academic Press, New York, 1970) pp. 293–417, appendies on pp. 515–568.
13. M. Van Thiel, ed., *Compendium of Shock Wave Data (Report UCRL-50108)* (Lawrence Livermore Lab., Livermore, 1977).
14. S. P. Marsh, ed., *LASL Shock Hugoniot Data* (Univ. of California Press, Berkeley, 1980).
15. R. F. Trunin, L. F. Gudarenko, M. V. Zhernokletov, and G. V. Simakov, *Experimental Data on Shock Compression and Adiabatic Expansion of Condensed Matter*, edited by R. F. Trunin (Russian Federal Nuclear Center VNIIEF, Sarov, 2001).
16. V. E. Fortov, "Extreme states of matter on earth and in space," Usp. Fiz. Nauk **179**, 653–687 (2009).
17. I. V. Lomonosov and S. V. Fortova, "Wide-range semiepirical equations of state of matter," High Temperature **55**, 585–610 (2017).
18. V. E. Fortov and I. V. Lomonosov, "Thermodynamics of extreme states of matter," Pure and Applied Chemistry **69**, 893–904 (1997).
19. I. V. Lomonosov, "Multi-phase equation of state for aluminum," Laser and Particle beams **25**, 567–584 (2007).
20. J. M. Walsh, M. H. Rice, R. G. McQueen, and F. L. Yarger, "Shock-wave compressions of twenty-seven metals. equations of state of metals," Physical Review **108**, 196–216 (1957).
21. L. V. Al'tshuler, K. K. Krupnikov, B. N. Ledenev, V. I. Zhuchikhin, and M. I. Brazhnik, "Dynamical compressibility and equation of state for iron under high pressure," Sov. Phys. — JETP **7**, 606–613 (1958).
22. L. V. Al'tshuler, K. K. Krupnikov, and M. I. Brazhnik, "Dynamical compressibility of metals under pressure from 400000 to 4 million atmospheres," Sov. Phys. — JETP **34**, 614–618 (1958).
23. S. B. Kormer, A. I. Funtikov, V. D. Urlin, and A. N. Kolesnikova, "Dynamical compression of porous metals and the equation of state with variable specific heat at high temperatures," Sov. Phys. — JETP **15**, 477–488 (1962).
24. L. V. Al'tshuler, A. A. Bakanova, I. P. Dudoladov, E. A. Dynin, R. F. Trunin, and B. S. Chekin, "Shock adiabatic curves for metals. New data, statistical analysis and general laws," Journal of Applied Mechanics and Technical Physics **22**, 145–169 (1981).
25. L. V. Al'tshuler, B. N. Moiseev, L. V. Popov, G. V. Simakov, and R. F. Trunin, "Relative compressibility of iron and lead at pressures of 31 to 34 Mbar," Sov. Phys. — JETP **27**, 420–422 (1968).
26. R. F. Trunin, M. A. Podurets, B. N. Moiseev, G. V. Simakov, and L. V. Popov, "Relative compressibility of copper, cadmium and lead at high pressures," Sov. Phys. — JETP **29**, 630–631 (1969).
27. A. S. Vladimirov, N. P. Voloshin, V. N. Nogin, A. V. Petrovtsev, and V. A. Simonenko, "Shock compressibility of aluminum at $p \geq 1$ Gbar," Sov. Phys. — JETP Lett. **39**, 85–88 (1984).
28. R. F. Trunin, M. A. Podurets, L. V. Popov, V. N. Zubarev, A. A. Bakanova, V. M. Ktitorov, A. G. Sevast'yanov, G. V. Simakov, and I. P. Dudoladov, "Measurement of the compressibility of iron at 5.5 TPa," Sov. Phys. — JETP **75**, 777–780 (1992).
29. R. F. Trunin, M. A. Podurets, L. V. Popov, B. N. Moiseev, G. V. Simakov, and A. G. Sevast'yanov, "Determination of the shock compressibility of iron at pressures up to 10 TPa (100 Mbar)," Sov. Phys. — JETP **76**, 1095–1098 (1993).
30. L. V. Altshuler, A. V. Bushman, M. V. Zhernokletov, V. N. Zubarev, A. A. Leont'ev, and V. E. Fortov, "Unload isentropes and equation of state of metals at high energy densities," Sov. Phys. — JETP **51**, 373–383 (1980).
31. Y. B. Zel'dovich and L. D. Landau, "Relation of the liquid to gaseous state at metals," Zh. Eksp. Teor. Fiz. **14**, 32 (1944).
32. E. Wigner, "On the interaction of electrons in metals," Phys. Rev. **46**, 1002 (1934).
33. G. E. Norman and A. N. Starostin, "Thermodynamics of a strongly nonideal plasma," High Temp. **8**, 381 (1970).
34. D. Saumon and G. Chabrier, "Fluid hydrogen at high density: The plasma phase transition," Phys. Rev. Lett. **62**, 2397 (1988).

35. C.-S. Yoo, N. C. Holmes, M. Ross, D. J. Webb, and C. Pike, "Shock temperature and melting of iron at Earth core conditions," Phys. Rev. Lett. **70**, 3931–3934 (1993).
36. G. R. Gathers, "Dynamic methods for investigating thermophysical properties of matter at very high temperatures and pressures," Rep. Progr. Phys. **49**, 341–396 (1986).
37. P. Renaudin, C. Blancard, J. Clerouin, G. Faussurier, P. Noiret, and V. Recoules, "Aluminum equation-of-state data in the warm dense matter regime," Phys. Rev. Lett. **91**, 075002–1–075002–4 (2003).
38. G. I. Kerley, "Theoretical equation of state for aluminum," International Journal of Impact Engineering **5**, 441 – 449 (1987).
39. D. A. Young and E. M. Corey, "A new global equation of state model for hot, dense matter," Journal of Applied Physics **78**, 3748–3755 (1995).
40. V. E. Fortov, V. V. Kim, I. V. Lomonosov, A. V. Matveichev, and A. V. Ostrik, "Numerical modeling of hypervelocity impacts," International Journal of Impact Engineering **33**, 244–253 (2006).
41. D. J. Liquornik and G. W. Pomykal, *Digitized data for Delco test 4007, lead-on-lead. Lawrence Livermore Laboratory Report DDV-86-0010* (Lawrence Livermore Laboratory, 1986).
42. K. S. Holian, "Hydrodynamics code calculations of debris clouds produced by ball-plate impacts," Int J Impact Engng , 231–239 (1990).
43. I. V. Lomonosov, A. V. Bushman, V. E. Fortov, and K. V. Khishenko, "Caloric equations of state of structural materials," in *HIGH-PRESSURE SCIENCE AND TECHNOLOGY - 1993, PTS 1 AND 2*, edited by Schmidt, S. C. and Shaner, J. W. and Samara, G. A. and Ross, M. (INT ASSOC RES & ADV HIGH PRESSURE SCI & TECHNOL; AMER PHYS SOC, TOPICAL GRP SHOCK COMPRESS CONDENSED MATTER, 1994) pp. 133–136, Joint Conference of the International-Association-for-Research-and-Advancement-of-High-Pressure- Science-and-Technology/American-Physical-Society-Topical-Group-on-Shock- Compression-of-Condensed-Matter, COLORADO SPRINGS, CO, JUN 28-JUL 02, 1993.